

Rheological and Mechanical Study of Micro-Nano Sized Biocarbon-PLA Biodegradable Biocomposites

Md. Rezaur Rahman,^{a,*} Al-Khalid Bin Othman,^a Yuriy Yurkin,^b Andrey Burkov,^b Ulyana Shestakova,^b Muhammad Khusairy Bin Bakri,^{a,c} Sulaiman Y. Alfaifi,^d O. Madkhali,^e Mahmood D. Aljabri,^f and Mohammed M. Rahman^g

Pinewood sawdust was pyrolyzed to create a micro-nanocarbon. The adsorbent's particle size was reduced during a ball milling procedure to improve the surface area and encourage porosity growth. The synergistic effects of micro-nano-adsorbent-reinforced poly(lactic acid) (PLA) composites were investigated by analyzing the efficiency of the rheological process. The properties of the prepared composites also were examined using various characterization tests, including tensile and hardness tests, crystallinity tests, elemental composition, and plasticity behavior tests. Therefore, in-depth investigations and comparisons were also carried out to confirm the created composites' efficacy compared to other outcomes.

DOI: 10.15376/biores.18.3.4492-4509

Keywords: Biocarbon; Pine; Mechanical properties; Rheology properties

Contact information: a: Faculty of Engineering, Universiti Malaysia Sarawak (UNIMAS), 94300 Kota Samarahan, Sarawak, Malaysia; b: Building Structures and Machines Department, Vyatka State University, 610020 Kirov, Russia; c: Composite Materials and Engineering Center, Washington State University, 2001 East Grimes Way, 99164, Pullman, Washington, U.S.A.; d: Department of Chemistry, King Abdulaziz University, Jeddah 21589, Saudi Arabia; e: Department of Physics, College of Science, Jazan University, P.O. Box 114, Jazan 45142, Kingdom of Saudi Arabia; f: Department of Chemistry, University College in Al-Jamoum, Umm Al-Qura University, Makkah 21955, Saudi Arabia; g: Center of Excellence for Advanced Materials Research (CEAMR), King Abdulaziz University, Jeddah 21589, Saudi Arabia;

* Corresponding author: rmrezaur@unimas.my

INTRODUCTION

The white pine group, *Pinus* subgenus *Strobus*, includes *Pinus sibirica*. All group members have leaves in fascicles (bundles) of five and have a deciduous sheath (Grandpre *et al.* 2011). They measure 5 to 10 cm. Pine cones from Siberia are 5 to 9 cm long. The solitary remaining wing on the 0.9 to 1.2 cm long seeds is used for dispersal by spotted nutcrackers. Some botanists consider the Siberian pine a variant or subspecies of the closely related Swiss pine (*Pinus cembra*) (Hohn *et al.* 2009). It differs from Swiss pine because it has more prominent cones and needles with three resin channels rather than just two. White pine blister rust does not affect Siberian pine nearly as much as other European and Asian white pines (*Cronartium ribicola*). This fungus was unintentionally brought from Europe to North America, where it has devastated native white pine trees throughout the continent, especially the closely related whitebark pine. Siberian pine is statistically significant for hybridization and genetic modification studies to create rust resistance in these species (Kuznetsova 2008; Alongi *et al.* 2019).

Materials formed from a mixture of biocarbon and other materials, such as plastic or metal, are known as biocarbon composites. Sustainability, carbon sequestration, mechanical qualities, biocompatibility, cost-effectiveness, biodegradability, and adaptability are just a few advantages they provide (Samir *et al.* 2022). Biocarbon composites can be more ecologically friendly than conventional composites since they are constructed from sustainable and biodegradable ingredients. As the biocarbon component of the composite stores carbon that would otherwise be released into the atmosphere, biocarbon composites may aid in removing carbon dioxide from the environment (Zhang *et al.* 2022). Biocarbon composites may have more robust and more rigid mechanical characteristics when compared to conventional composites. Because they are biocompatible, biocarbon composites may be employed in medical applications (Bartoli *et al.* 2022). Compared to standard composites, biocarbon composites are more affordable because they may be made from agricultural waste and other inexpensive feedstocks. Biocarbon composites may reduce environmental harm by reducing garbage dumped in landfills. Applications for biocarbon composites include consumer items, packaging, transportation, and construction (Shanmugam *et al.* 2021).

Nagarajan *et al.* (2016) used biocarbon as a renewable carbonaceous filler for engineering plastic composites. The mixing matrix was poly(trimethylene terephthalate) (PTT), polylactic acid (PLA), and terpolymer. Biocarbon filler was separated by particle size. The composite microstructure would be changed with the biocarbon particle size and aspect ratio (Nagarajan *et al.* 2016). Composites with a biocarbon particle size range of 20 to 75 μm were found to have more excellent blend component dispersion. Rheological measurements showed that biocarbon enhanced viscosity but conserved matrix shear-thinning (Nagarajan *et al.* 2016). The cited authors found that biocarbon with proper particle sizes and processing aids and conditions regulating morphology and crystallinity may yield composites with improved mechanical and thermal performance. Research by Snowdon *et al.* (2019) examined the impacts of talc and two sizes of biocarbon as fillers in a PLA bioplastic. Due to their high rigidity, the compression molded sheets demonstrated a higher than 69% decrease in abrasion compared to the clean PLA. Only talc, in contrast, has the barrier qualities that prevent both water and oxygen penetration, and biocarbon lacks the high aspect ratio required to create the necessary winding route for barrier enhancement (Snowdon *et al.* 2019). The char-like nature of the biocarbon-filled PLA biocomposites allowed them to outperform the clean PLA and talc variation; however they failed the horizontal burning test regarding flammability resistance (Snowdon *et al.* 2019). The presence of the biocarbon, which did not happen with the talc, caused the PLA chains to degrade, as seen by the rheology of the composites, which may also have led to the lower barrier and more excellent burn resistance from increased dripping (Snowdon *et al.* 2019).

As a result, this study aims to pyrolyze pine wood sawdust to produce a micro-nanocarbon. The adsorbent's particle size was decreased during the ball milling process to increase surface area and promote porosity development. Analyzing the effectiveness of the rheological process makes it possible to investigate the synergistic impacts of micro-nano-adsorbent-reinforced PLA biocomposites. The properties of the prepared composites have also been investigated using several characterization tests, such as Scanning Electron Microscopy (SEM) with Energy Dispersive X-ray Spectroscopy (EDX), Differential Scanning Calorimetry (DSC), Thermogravimetric Analysis (TGA), mechanical tests, and hardness tests, by observing the crystallinity, morphological images, as well as the elemental composition and plasticity behavior of the composite. In-depth studies and

comparisons are also conducted to verify the generated composites' effectiveness compared to other outcomes.

EXPERIMENTAL

Materials

The film-grade poly(lactic) acid (Product No. PLA4042D) was supplied by NatureWorks, USA. The pine sawdust was provided by Vyatka State University, Kirov, Russia. Ethanol brand «Extra» (National Standard of RF 55878-2013 Rectified hydrolytic technical ethyl alcohol. Specifications) was provided by Kirov BioChemical Plant Ltd, Russia.

Methods

Preparation of wood biomass

The sawdust from pine trees was ground into fine particles using a Panasonic MX-AC 400 Mixer/Grinder (Panasonic Corporation, Kadoma, India). The sample was then sieved through a 900 µm sieve to get particles of the same micrometer size, and it was kept in a dry, room-temperature environment for later usage, as seen in Fig. 1.



Fig. 1. The sieved ground pine particles

Chemical activation of wood fine particles

0.05M of dilute acetic acid solution was used for chemical activation to ensure a suitable porosity level in the activated biocarbon. Figure 2 shows that the fine pine particle was immersed in the mixture and slowly stirred for one and a half hours. After activation, the sample was filtered and neutralized with distilled water before being dried in an oven (BF Avantgarde - Model BF 56 - BINDER Asia Pacific (Hong Kong) Ltd.) for 48 hours at 60 °C before carbonization. The sample was spread around the plate's flat surface to ensure the heat was dispersed equally. Additionally, this gets rid of the unpredictable hotspots used for drying.



Fig. 2. The chemical activation process

Wood fine particle carbonization

Utilizing an LT Furnace (Control Therm Sdn. Bhd.), the carbonization process was carried out. As shown in Fig. 3, the dried treated wood particle was then put into a ceramic bowl, coated in aluminum foil, and covered in a layer of clay before carbonization to avoid sample oxidation. It was then put into the LT furnace to undergo carbonization. The temperature was escalated throughout the carbonization process from room temperature to 200 °C and subsequently to 400 °C with a heating rate of 10 °C/min. The temperature was maintained at 400 °C for an hour, so carbonization could occur. The furnace was cooled until it reached room temperature at a rate of 6.16 °C/min. The sample was placed in a furnace overnight and taken out the next day. The graph of the carbonization process's time setting is shown in Fig. 4. The fine biocarbon was produced after the carbonization procedure, as illustrated in Fig. 5. To further decrease the size of fine biocarbon and aid the ball milling process, it was gathered and sieved using a 200 µm sieve.



Fig. 3. The fine wood particle was covered in clay to shield it from oxides

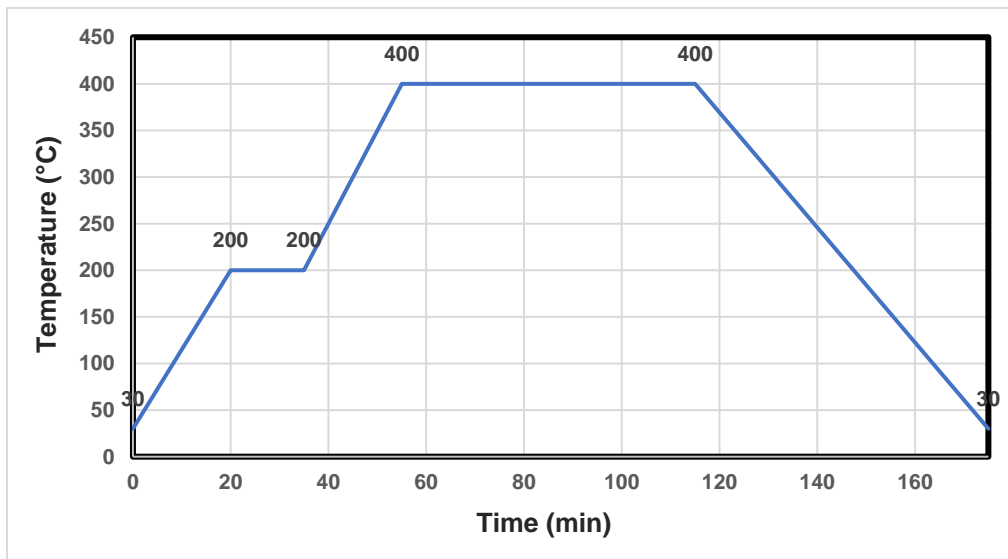


Fig. 4. Time setting for LT furnace



Fig. 5. The carbonization process of biocarbon is produced before the ball-milled process

Ball milling process to obtain the micro-nanocarbon

The Retsch ball milling apparatus (Model PM400 - Retsch GmbH, Haan, Germany), which is shown in Fig. 6(a), was used to create nanoscale biocarbon (or biochar). The produced coarse biocarbon was processed using a grinder for around 5 to 10 minutes at a speed range from 18,000 to 20,000 rpm to help the ball milling process. Initiating the ball milling procedure was fine-ground biocarbon. It was added to the ball mill's cylindrical compartment, around 55% of its total capacity. The procedure used 20 stainless steel balls weighing 0.5 g each to reduce the biochar to nano size. The micro-nano-size level was achieved when the tiny biocarbon particle was ground for 30 hours, and a sample was regularly taken for testing. The fine micro-nano-size biocarbon after ball milling is shown in Fig. 6(b).

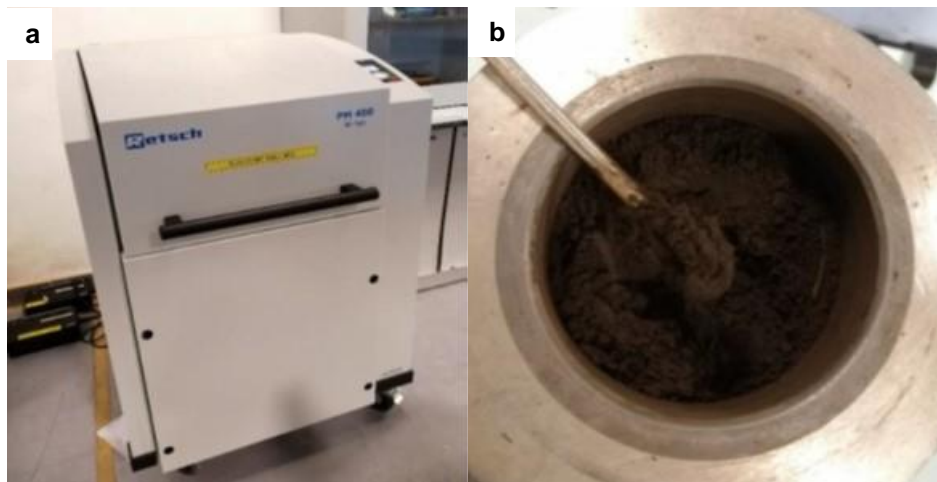


Fig. 6. (a) A Retsch ball milling machine and (b) micro-nano-sized biocarbon after ball milling was used

Compounding the biocomposites

For compounding, the raw biocarbon was furthered process with a Planetary Ball Mill PM 100 (Retsch GmbH, Haan, Germany) using two methods; dry (biocarbon A) and wet (biocarbon B). Biocarbon A was ball-milled in a dried condition, and biocarbon B used ethanol as a lubricant.

In melt mixing (MM), the processed biocarbon powder was compounded with the PLA4042D matrix using a Brabender Plastograph (France) mixer and operating at 170 °C, 100 rpm for 10 min. Neat PLA was subjected to the same processing. 0% (neat PLA), 0.5%, 1.0%, 2.5%, and 5.0%, of biocarbon-PLA were made. Two biocarbon products were made with the raw sample. Test specimens were obtained by injection molding at 180°C.

Testings and Characterizations

Particle size distribution (PSD)

The particle size distribution test was done according to ASTM D1921-18 (2018). The test used various sieves chosen to cover the materials' particle sizes. The mean particle diameter and particle size distribution were calculated using this approach.

Rheological test

This test was done according to ASTM D4440-08 (2015) on a RHEOLOGICA device (Sweden). The rheological properties of the composites were taken from a logarithmic frequency of 0.01 to 100. The testing temperature was 170 °C. It may be used to determine the complex viscosity and other significant viscoelastic characteristics of such materials as frequency, strain amplitude, temperature, and time. Such properties may be influenced by fillers and other additives. Parallel plate geometry was adopted, with a diameter of 20 mm and a gap of 1 mm.

Tensile test

The tensile tests were carried out according to the ASTM D638-14 (2022) standard on the testing machine Autograph AG-X 5kN (Shimadzu (Japan) Corp.) at the crosshead speed of 100 mm/min. The thickness of the sample was 2 mm. An average value of five specimens for each weight percentage was calculated.

Hardness test

The specimen is first placed on a hard flat surface according to ASTM D2240-15 (2021). The test specimens are generally 6.4 mm thick. The indenter for the instrument was then pressed into the specimen, ensuring that it was parallel to the surface. The hardness was read within one second of firm contact with the specimen. The Shore D Hardness Scale is usually used to measure the hardness of rubber, semi-rigid, and hard plastics.

Scanning electron microscopy (SEM) and energy dispersive X-Ray spectroscopy (EDX/EDS)

The morphological images of the samples, especially the pore or size of the structure, were evaluated *via* Hitachi analytical tabletop SEM (benchtop) (TM-3030, Hitachi High Technologies, Mannheim, Germany). The specimens were mounted on aluminum stubs and were fine-coated using auto fine coater JFC-1600 (Jeol, Tokyo, Japan). The morphological images of the sample were captured using a field emission gun with an acceleration voltage of 5 and 15 kV. EDX analysis was used to determine the elementary material composition present on the surface of the samples, which was correlated with SEM images produced for the individual specimen. The procedure for the SEM analysis was conducted following the ASTM E2015-04 (2021) standards.

Thermogravimetric analysis (TGA)

TGA analysis was performed on a DTG-60 (Shimadzu (Japan) Corp.) workstation analyzer. The sample was heated at 10 °C/min under flowing nitrogen (150 mL/min) at 30 to 600 °C. It was conducted under the ASTM E1868-10 (2021) and ASTM E1131-20 (2020) standards.

Differential scanning calorimetry (DSC)

The differential scanning calorimetry (DSC) analysis was performed on the DSC-60 (Shimadzu (Japan) Corp.). The specimens were examined under flowing nitrogen (20 mL/min) over a temperature range of 30 to 200 °C (heating rate of 10 °C/min). The test was repeated a few times for each sample, and the most representative precise results were used. It was done according to ASTM D3418-15 (2021) and ASTM E1269-11 (2018) standards.

RESULTS AND DISCUSSION

Particle Size Distribution

Figures 7 and 8 show the integral and differential curves of the numerical particle distribution of biocarbon types A (dry) and B (wet). The graph shows that the diameter size of biocarbon A dry was higher than that of biocarbon B for both integral and differential curves of the numerical particle size distribution. The graphs also showed that biocarbon B had more nanoparticles than biocarbon A. Dry ball milling creates more coarse surfaces than wet ball milling, which is finer. However, it depends on the ball used during milling (Kumar *et al.* 2018). Wet milling usually produces fine higher quality, while dry milling produces coarse low quality (Munhkbayar *et al.* 2013). However, wet milling requires lubricant or enhancement, which consumes more energy (Munhkbayar *et al.* 2013).

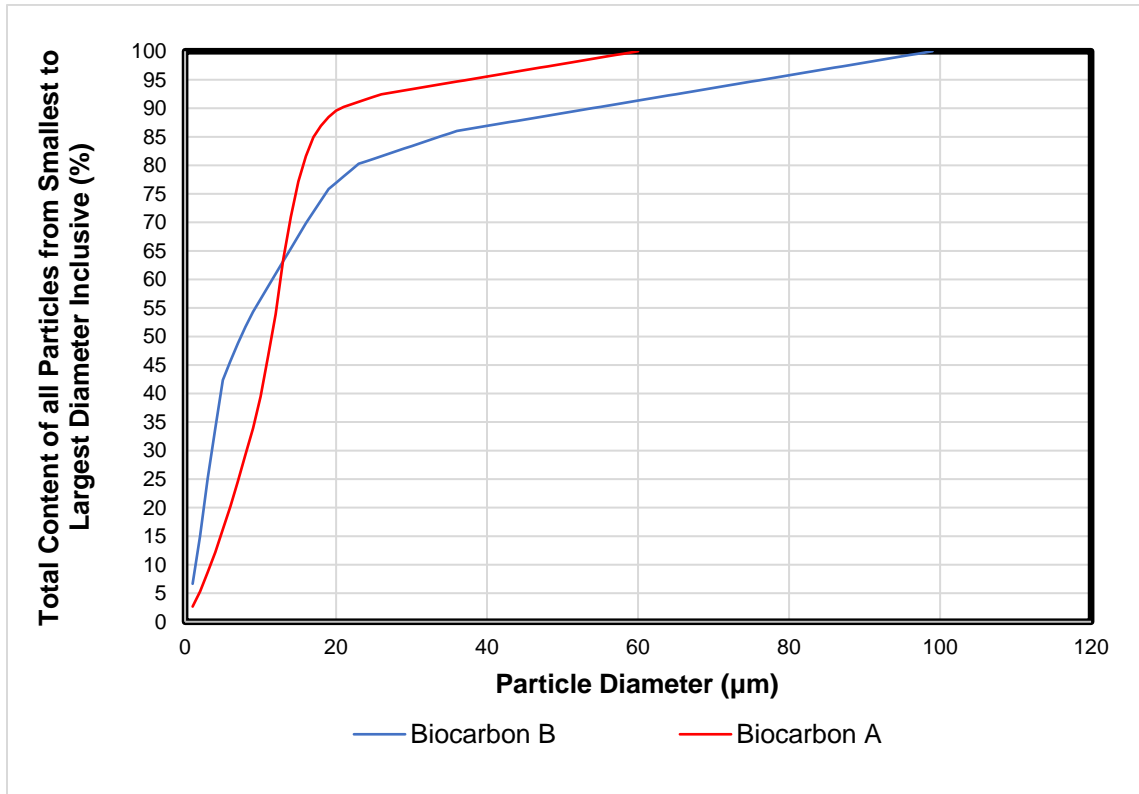


Fig. 7. Integral curve of the numeral particle distribution of biocarbon A (dry) and B (wet)

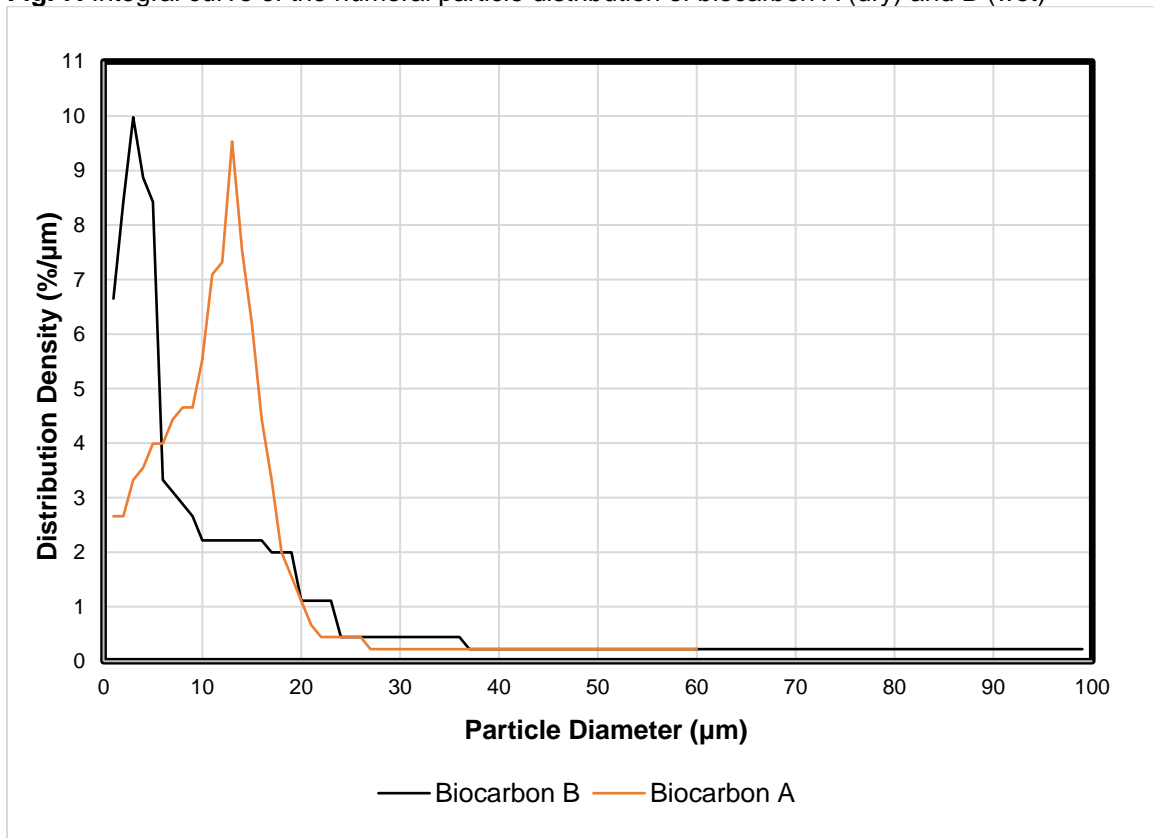


Fig. 8. Differential curve of the numeral particle distribution of biocarbon A (dry) and B (wet)

Morphological and Elemental Properties

Figure 9 shows an image of raw biocarbon at magnifications of x100 and x250. Figures 9 and 10 show an image of biocarbon A and biocarbon B at magnifications of x250, x500, x1000, x2500, and x5000. Figures 10 and 11 show that the particle size was reduced as a result of the ball milling. However, Fig. 11 shows the biocarbon B particle was finer than Fig. 10 for biocarbon A. The reason behind this was the wet conditions, where ethanol is used as a lubricant, which allowed the particle size to be reduced. However, it is noticed that the particles agglomerated with each other due to electrostatic force as the size was reduced (Endres *et al.* 2021).

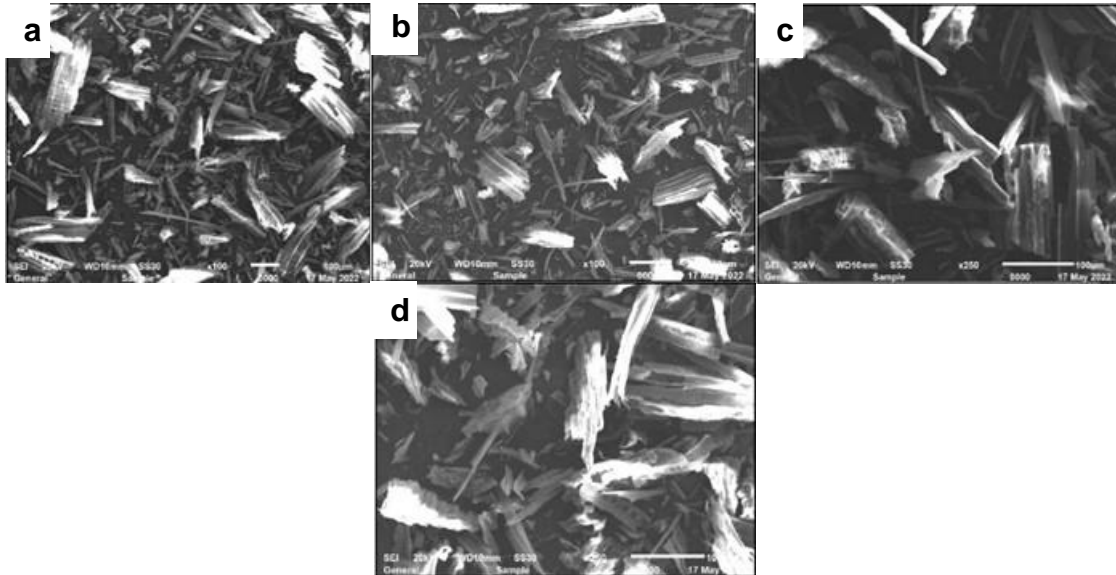


Fig. 9. SEM of raw biocarbon of (a) and (b) is at x100, and (c) and (d) is at x250

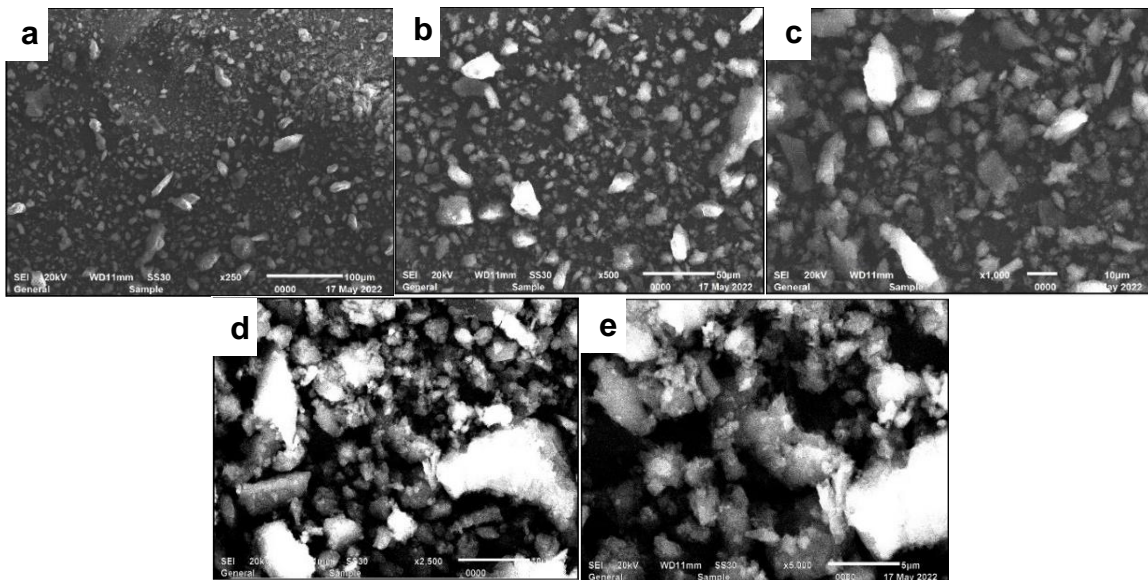


Fig. 10. SEM images of biocarbon A at (a) 250, (b) 500, (c) 1000, (d) 2500, and (e) 5000

It is also noticed that some of the particle sizes of biocarbon B were less small than biocarbon A, which is in the nanoscale. However, small parts of the biocarbon B still were

microsize due to the ball milling duration, which was very short, and also due to agglomeration between biocarbon due to electrostatic forces (Panigrahi *et al.* 2018). Table 1 shows the EDS/EDX result of the biocarbon.

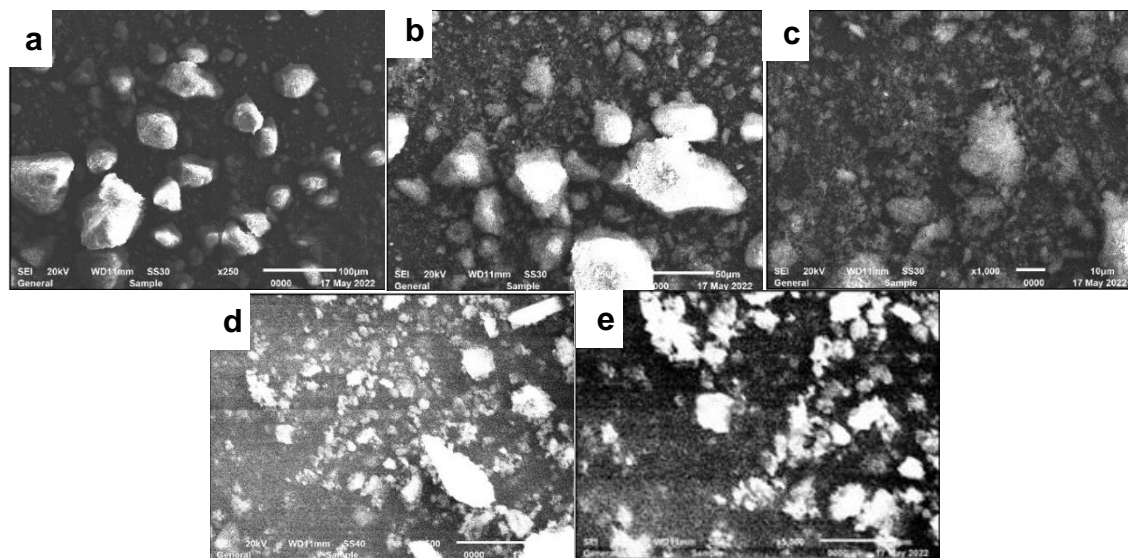


Fig. 11. SEM images of biocarbon B at (a) 250, (b) 500, (c) 1000, (d) 2500, and (e) 5000

Table 1. Elemental Analysis of the Biocarbon

Elements	Mass (%)	Mass Normal (%)	Atom (%)
Carbon (C)	56.00	56.00	62.90
Oxygen (O)	44.00	44.00	37.10

Mechanical Properties (Hardness and Tensile)

Table 2 shows the hardness properties of biocarbon A-PLA and biocarbon B-PLA biocomposites. Hardness shore D means that the samples are determined as hard and semi-rigid. The addition of biocarbon in the PLA increased the surface hardness of the biocomposites. Biocarbon A and B fell in the extra hard range scale for Shore D classification. Both biocarbon-PLA composites showed extra hard properties with little flexibility (Li *et al.* 2020). Figure 12 shows the biocarbon A-PLA and biocarbon B-PLA biocomposite tensile strength. It is apparent that the 1 wt% of biocarbon B had the highest tensile strength, 61 MPa. The addition of biocarbon increased the tensile strength until it reached the optimum strength. It started to loosen its strength after 1 wt% due to over-saturation, leading to decreased interfacial bond strength (Jubinville *et al.* 2019). Other reasons are the biocarbon pore structure, distribution, and chemical reactions between biocarbon and PLA (Behazin *et al.* 2017).

Table 2. The Hardness – Shore D of Biocarbon-PLA Biocomposites

Ball Milling Condition	Weight Percentage of Biocarbon				
	0.0	0.5	1.0	2.5	5.0
Biocarbon A (Dry)	75	81	81	80	81
Biocarbon B (Wet)		81	80	80	80

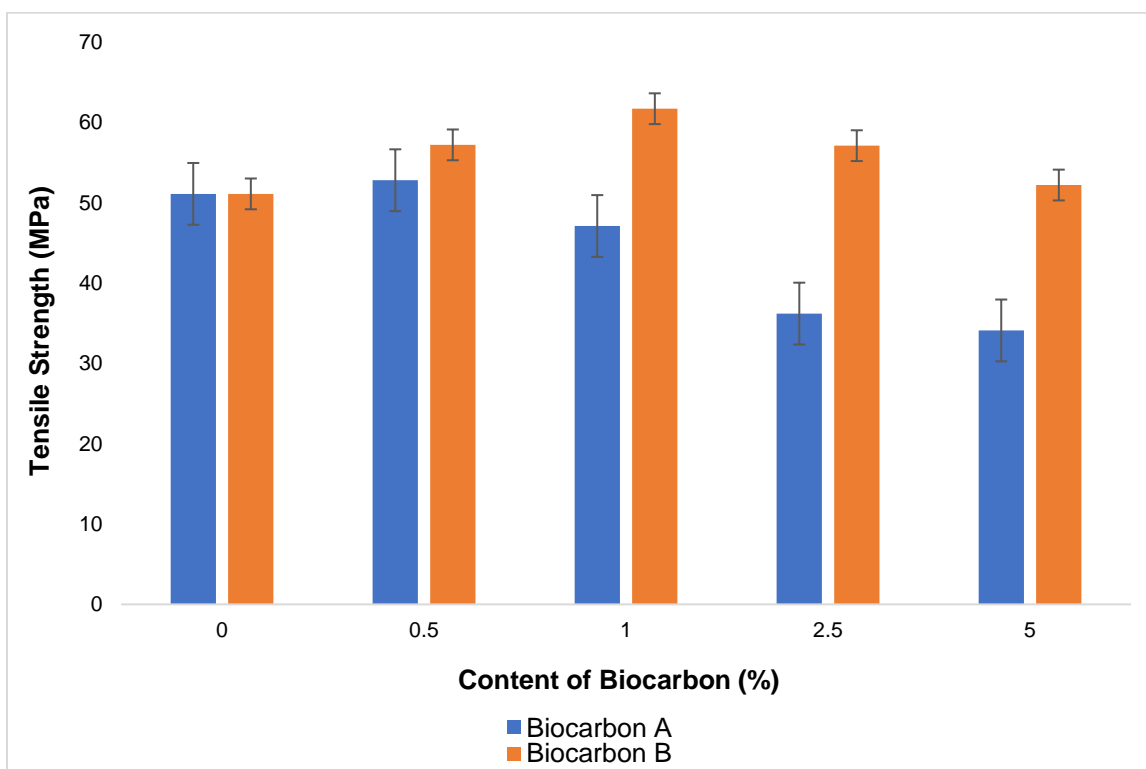


Fig. 12. Tensile properties of biocarbon A- and B-PLA biocomposites

Thermal Properties

Table 3 and Fig. 12 show the DSC of biocarbon B-PLA biocomposites. The DSC results of the biocarbon B-PLA biocomposites indicate that the percentage of crystallinity was reduced as it increased in biocarbon content, making it more amorphous. The reason behind this was due to the disorderly structure of biocarbon B. Another reason was that the biocarbon particles are often irregular in shape and size, and they disordered the molecular chains in the polymer matrix of the biocomposites (Ogunsona *et al.* 2017). The effect may also be due to interfacial interaction between biocarbon particles and PLA. The formation of chemical bonds between two phases, such as hydrogen bonding, can hinder the formation of crystalline structures. Lastly, the processing condition of the biocarbon-PLA biocomposites, such as temperature, may have affected the outcomes.

Table 3. DSC of Biocarbon B-PLA Biocomposites

Weight Percentage of Biocarbon	T_g (°C)	T_c (°C)		T_m (°C)		Percentage of Crystallinity (%)
		Peak	Heat (J/g)	Peak	Heat (J/g)	
BC 0	60.46	111.93	25.78	155.82	27.77	18
BC 0.5	61.53	122.19	18.59	152.74	21.05	14
BC 1	61.80	122.10	17.21	152.82	20.55	14
BC 2.5	62.34	129.69	9.43	155.55	9.93	7
BC 5	61.46	129.03	6.17	153.6	9.03	6

Table 4 and Fig. 13 show the TGA results of biocarbon B-PLA biocomposites. As a rule of thumb, with consideration of the DSC, having a higher percentage of crystallinity with a higher amount of biocarbon, biocarbon B-PLA biocomposites with 1.0 wt% were considered to have a great advantage compared to 0.5 wt%, as it was able to store more biocarbon and in addition, having a higher TGA thermal stability compared to others.

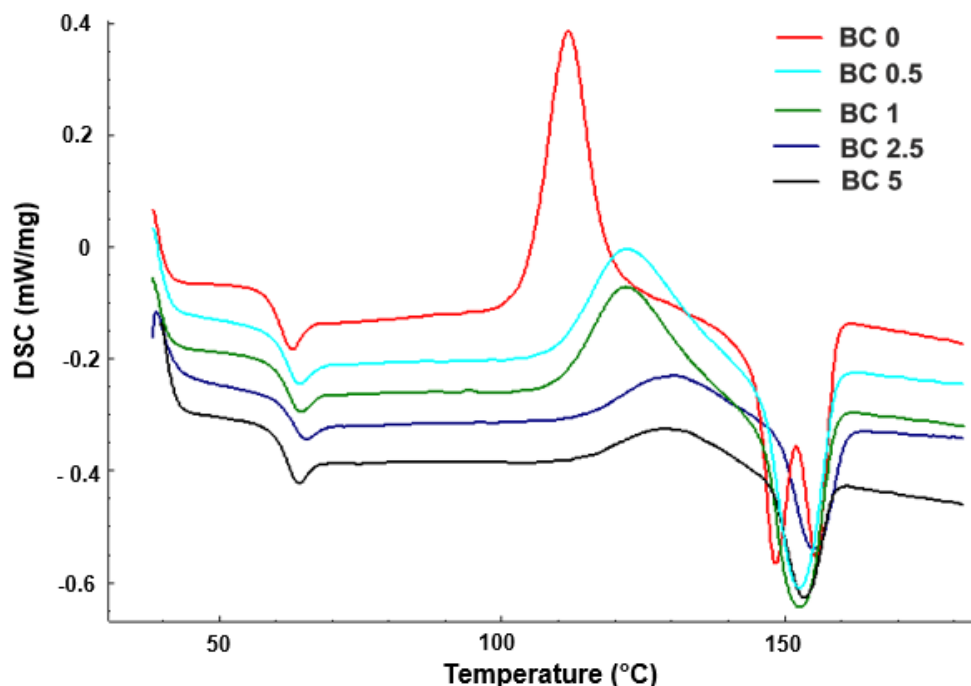


Fig. 13. DSC-thermograms of biocarbon B-PLA biocomposites

Table 4 and Fig. 13 show the TGA of biocarbon B-PLA biocomposites.

Table 4. Biocarbon B Influence in the Biocomposites

Percentage of Biocarbon	1%	3%	5%	10%	50%	90%
BC 0	292.38	296.77	314.19	329.16	356.3	372.66
BC 0.5	297.47	310.22	317.63	329.33	356.36	376.83
BC 1	293.15	311.04	319.5	329.64	355.39	378
BC 2.5	228.45	307.47	314.95	326.48	355.19	375.1
BC 5	293.55	314.82	322.78	331.29	356.4	391.34

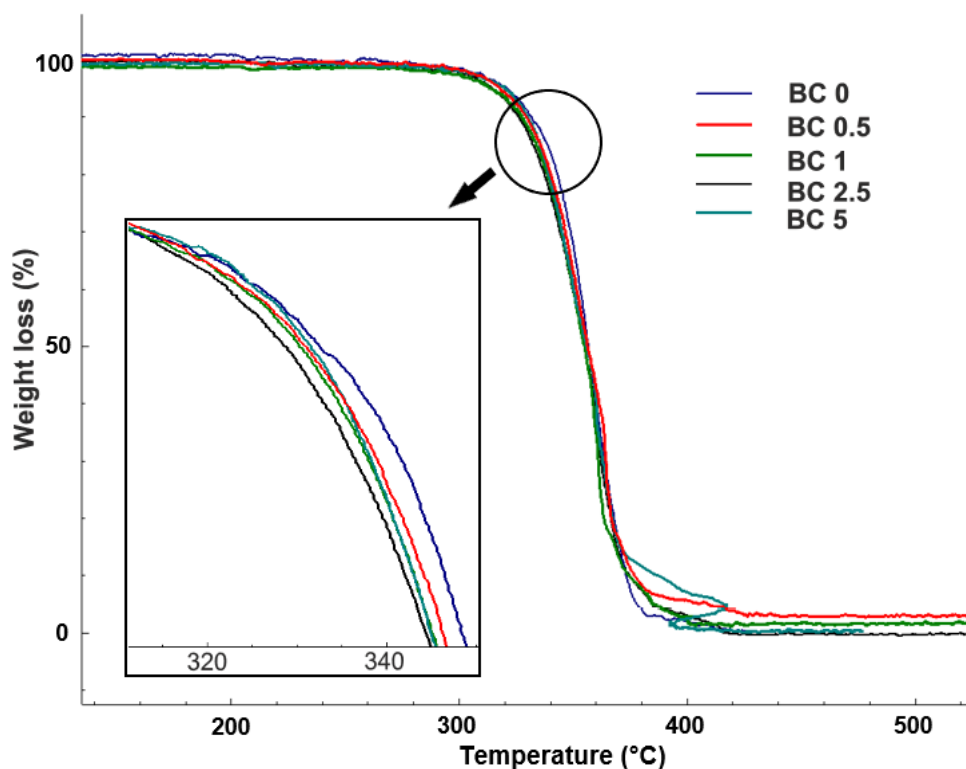


Fig. 14. TGA graphs of biocarbon B-PLA biocomposites

Rheological Properties

Figures 14, 15, and 16 show the biocarbon B-PLA biocomposites' log viscosity, storage modulus, and loss modulus. The graph shows that 1 wt% of BC had the highest log viscosity, storage modulus, and loss modulus values.

Figure 14 shows that the biocarbon B-PLA biocomposites sample was fluid and self-leveling, with a zero-shear viscosity plateau. It also shows that the polymer's viscosity decreased as the shear stress rate increased. In other words, when a shear force is applied, its viscosity decreases, making it easier to flow (Wilkes 1981).

Such behavior is often associated with the presence of a suspension or emulsion (Wilkes 1981). Above log frequency at 1, the biocomposites exhibited a shear-thinning phenomenon.

Figures 15 and 16 show more dissipative activity than elastic behavior, as the loss modulus was larger than the storage modulus. In other words, the system returned less energy and lost more energy as heat throughout the loading and unloading cycles (Mezger 2014).

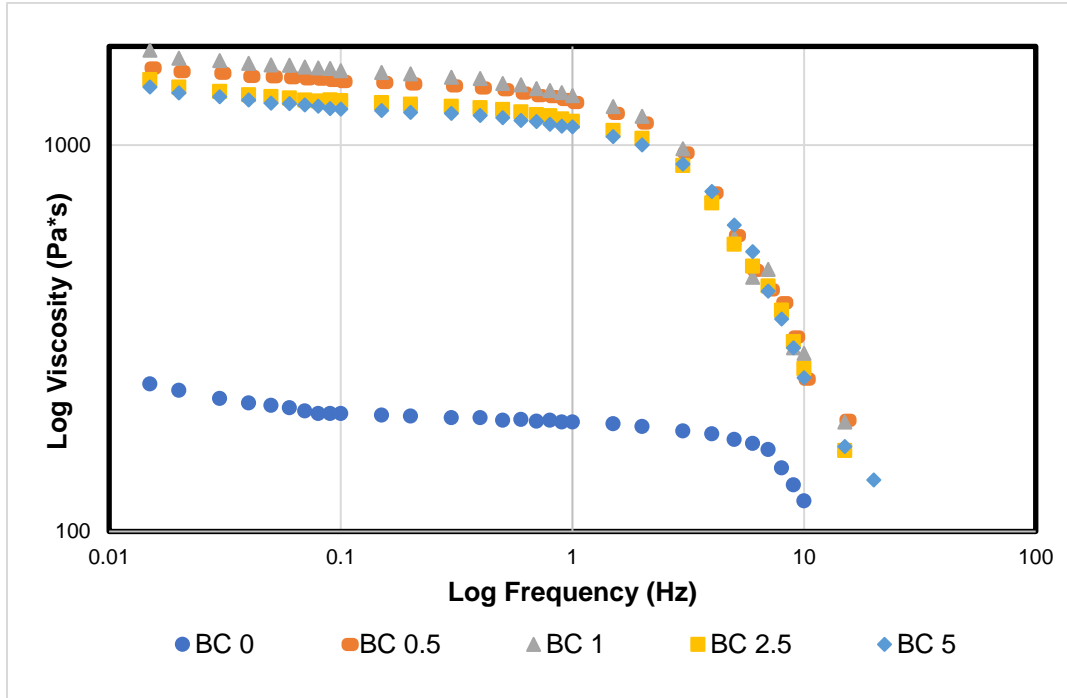


Fig. 15. Log viscosity graph of biocarbon B-PLA biocomposites

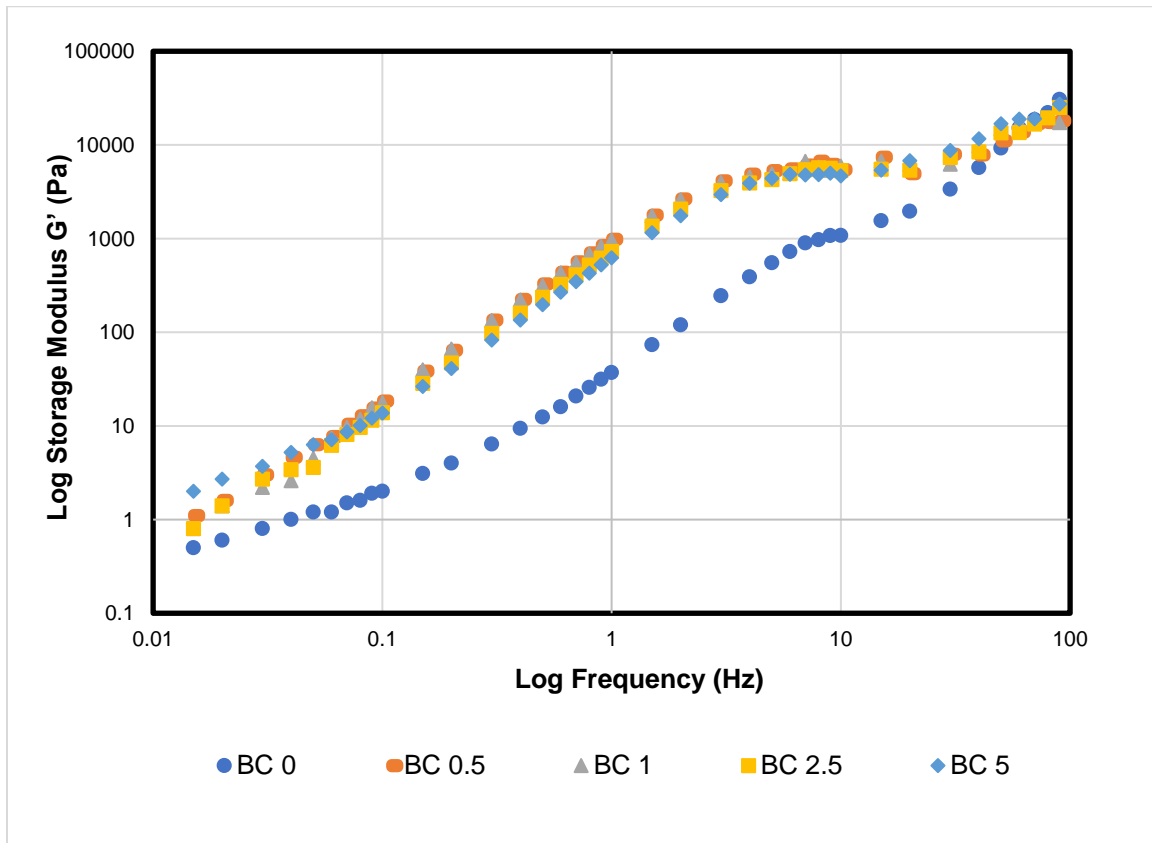


Fig. 16. Log storage modulus graph of biocarbon B-PLA biocomposites

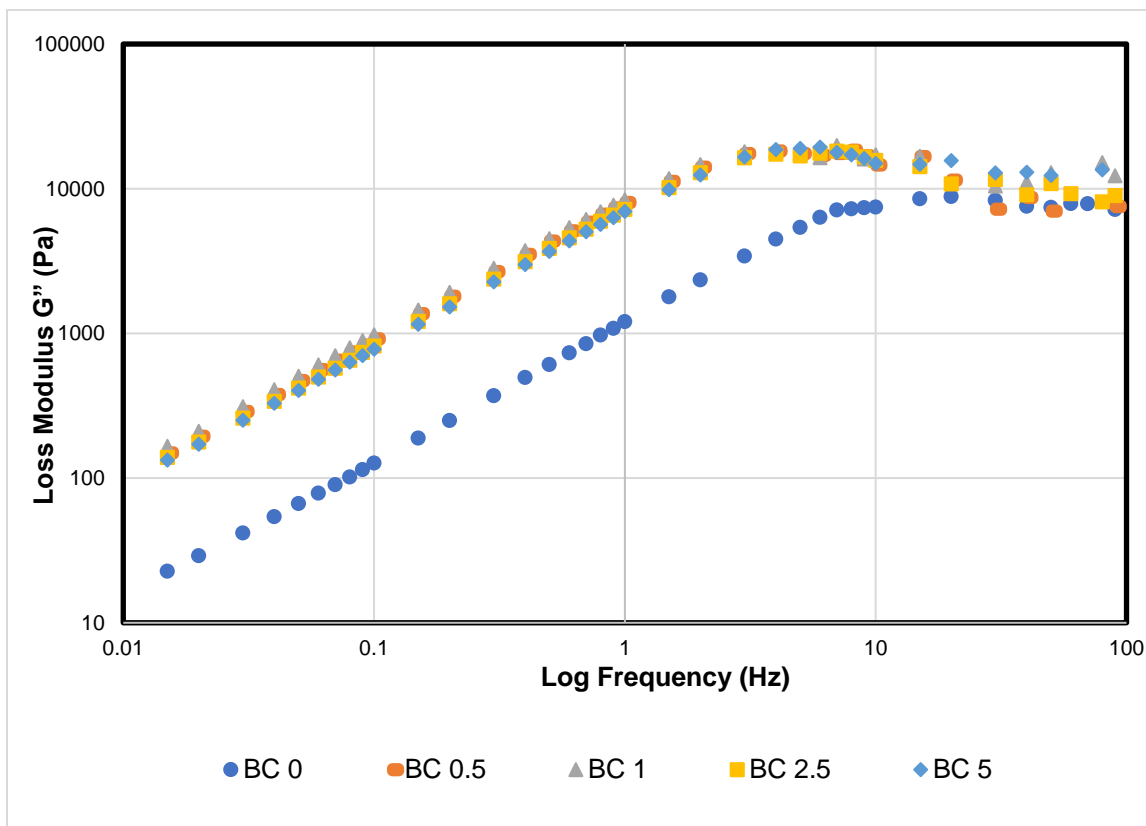


Fig. 17. Log loss modulus graph of biocarbon B-PLA biocomposites

CONCLUSIONS

1. Integral and differential curves of the numerical particle distribution showed the biocarbon A and biocarbon B particle diameter. According to the finding, the average particle diameter of biocarbon B was smaller. However, biocarbon A had larger amounts of nano-sized particles than micro-sized particles.
2. Morphological images show that the biocarbon B particles tended to agglomerate with each other. This was attributed to the nano-micro dimensions of the biocarbon and electrostatic forces. Elemental analysis showed that carbon and oxygen were the main components of the biocarbon.
3. The addition of biocarbon A and B in the PLA to form biocomposites made the properties of the biocomposites extra hard with little flexibility, and the tensile strength increased at a certain point before losing its mechanical properties.
4. From the perspective of thermal properties of the biocarbon biocomposites, it was found that as the biocarbon content rose, the percentage of crystallinity decreased, making the material more amorphous.
5. The loss modulus was greater than the storage modulus, and the rheological characteristics of the biocomposites exhibited more dissipative activity than elastic behavior. In other words, the material returned less energy and expended more energy as heat throughout the loading and unloading processes.

ACKNOWLEDGMENTS

This research work was funded by Institutional Fund Projects under grant no (IFPIP-540-130-1443). The authors gratefully acknowledge technical and financial support provided by the Ministry of Education and King Abdulaziz University, DSR, Jeddah, Saudi Arabia.

REFERENCES CITED

- Alongi, F., Hansen, A. J., Laufenberg, D., Keane, R. E., Legg, K., and Lavin, M. (2019). "An economical approach to distinguish genetically needles of limber from whitebark pine," *Forests* 10(12), 1-10. DOI: 10.3390/f10121060
- ASTM D1921-18 (2018). "Standard test methods for particle size (sieve analysis) of plastic materials," ASTM International, West Conshohocken, PA.
- ASTM D22240-15 (2021). "Standard test method for rubber property—Durometer hardness," ASTM International, West Conshohocken, PA.
- ASTM D3418-21-14 (2021). "Standard test method for transition temperatures and enthalpies of fusion and crystallization of polymers by differential scanning calorimetry," ASTM International, West Conshohocken, PA.
- ASTM D4440-08 (2015). "Standard test method for plastics: Dynamic mechanical properties melt rheology," ASTM International, West Conshohocken, PA.
- ASTM D638-14 (2022). "Standard test method for tensile properties of plastics," ASTM International, West Conshohocken, PA.
- ASTM D1131-20 (2022). "Standard test method for compositional analysis by thermogravimetry," ASTM International, West Conshohocken, PA
- ASTM D1269- (2018). "Standard test method for determining specific heat capacity by differential scanning calorimetry," ASTM International, West Conshohocken, PA.
- ASTM D1868-10 (2021). "Standard test methods for loss-on-drying by thermogravimetry," ASTM International, West Conshohocken, PA
- ASTM E2015-04 (2021). "Standard guide for preparation of plastics and polymeric specimens for microstructural examination," ASTM International, West Conshohocken, PA.
- Bartoli, M., Arrigo, R., Malucelli, G., Tagliaferro, A., and Duraccio, D. (2022). "Recent advances in biochar polymer composites," *Polymer* 14(12), 1-15. DOI: 10.3390/polym14122506
- Behazin, E., Misra, M., and Mohanty, A.K. (2017). "Sustainable biocarbon from pyrolyzed perennial grasses and their effects on impact modified polypropylene biocomposites," *Composites Part B: Engineering* 118(1), 116-124. DOI: 10.1016/j.compositesb.2017.03.003
- Endres, S. C., Ciacchi, L. L., and Madler, L. (2021). "A review of contact force models between nanoparticles in agglomerates, aggregates, and films," *Journal of Aerosol Science* 153(1), 1-20. DOI: 10.1016/j.jaerosci.2020.105719
- Grandpre, L. D., Tardif, J. C., Hessel, A., Pederson, N., Conciatori, F., Green, T. R., Oyunsanaa, B., and Baatarbileg, N. (2011). "Seasonal shift in the climate responses of *Pinus sibirica*, *Pinus sylvestris*, and *Larix sibirica* trees from semi-arid, north-central Mongolia," *Canadian Journal of Forest Research* 41(6), 1242-1255. DOI: 10.1139/X11-051

- Hohn, M., Gugerli, F., Abran, P., Bisztray, G., Buonamici, A., Cseke, K., Hufnagel, L., Quintela-Sabaris, C., Saabastini, F., and Vendramin, G. G. (2009). "Variation in the chloroplast DNA of swiss stone pine (*Pinus cembra* L.) reflects contrasting post-glacial history of populations from the Carpathians and the Alps," *Journal of Biogeography* 36(9), 1798-1806. DOI: 10.1111/j.1365-2699.2009.02122.x
- Jubinville, D., Abdelwahab, M., Mohanty, A. K., and Misra, M. (2019). "Comparison in composite performance after thermooxidative aging of injection molded polyamide 6 with glass fiber, talc, and a sustainable biocarbon filler," *Journal of Applied Polymer Science* 137(17), 1-15. DOI: 10.1002/app.48618
- Kumar, D. S., Kumar, B. J., and Mahesh, H. M. (2018), "Quantum nanostructures (QDs): An overview," in: *Synthesis of Inorganic Nanomaterials: Advances and Key Technologies*, Woodhead Publishing, United Kingdom, Sawston, pp. 59-88. DOI: 10.1016/B978-0-08-101975-7.00003-8
- Kuznetsova, G. V. (2008). "Experiment of intraspecific hybridization of Siberian stone pine (*Pinus sibirica* Du Tour) clones in middle Siberia," *Eurasian Journal of Forest Research* 11(2), 87-87. <http://hdl.handle.net/2115/35365>
- Li, S., Xu, Y., Jing, X., Yilmaz, G., Li, D., and Turng, L.-S. (2020). "Effect of carbonization temperature on mechanical properties and biocompatibility of biochar/ultra-high molecular weight polyethylene composites," *Composites Part B: Engineering* 196(1), 1-15. DOI: 10.1016/j.compositesb.2020.108120
- Mezger, T. G. (2014). "Applied rheology with Joe Flow on rheology road," Anthon Paar GmbH, pp.1-191.
- Munhkbayar, B., Nine, M. J., Jeoun, J., Bat-Erdene, M., Chung, H., and Jeong, H. (2013). "Influence of dry and wet ball milling on dispersion characteristics of the multi-walled carbon nanotubes in aqueous solution with and without surfactant," *Powder Technology* 234(1), 132-140. DOI: 10.1016/j.powtec.2012.09.045
- Nagarajan, V., Mohanty, A. K., and Misra, M. (2016). "Biocomposites with size-fractionated biocarbon: Influence of the microstructure on macroscopic properties," *ACS Omega* 1(4), 636-647. DOI: 10.1021/acsomega.6b00175
- Ogunsona, E. O., Misra, M., and Mohanty, A. K. (2017). "Impact of interfacial adhesion on the microstructure and property variations of biocarbons reinforced nylon 6 biocomposites," *Composites Part A: Applied Science and Manufacturing* 98(1), 32-44. DOI: 10.1016/j.compositesa.2017.03.011
- Panigrahi, N., Chaini, R., Nayak, A., and Mishra, P. C. (2018). "Impact of milling time and method on particle size and surface morphology during nano particle synthesis from α -Al₂O₃," *Materials Today: Proceedings* 5(9), 20727-20735. DOI: 10.1016/j.matpr.2018.06.457
- Samir, A., Ashour, F. H., Abdel Hakim, A. A., and Bassyouni, M. (2022), "Recent advances in biodegradable polymers for sustainable applications," *NPJ Materials Degradation* 6(1), 1-10. DOI: 10.1038/s41529-022-00277-7
- Shanmugam, V., Mensah, R. A., Forsth, M., Sas, G., Restas, A., Addy, C., Xu, Q., Jiang, L., Neisiany, R. E., Singha, S., George, G., Jose, T., Berto, F., Hedenqvist, M. S., Das, O., and Ramakrishna, S. (2021). "Circular economy in biocomposite development: State-of-the-art, challenges and emerging trends." *Composite Part C: Open Access* 5(1), 1-20. DOI: 10.1016/j.jcomc.2021.100138

Snowdon, M. R., Wu, F., Mohanty, A. K., and Misra, M. (2019). “Comparative study of the extrinsic properties of poly(lactic acid)-based biocomposites filled with talc versus sustainable biocarbon,” *RSC Advances* 9(1), 6752-6761. DOI: 10.1039/C9RA00034H

Wilkes, G. L. (1981). “An overview of the basic rheological behavior of polymer fluids with an emphasis on polymer melts,” *Journal of Chemical Education* 58(11), 880-892. DOI: 10.1021/ed058p880

Zhang, Y., He, M., Wang, L., Yan, J., Ma, B., Zhu, X., OK, Y. S., Mechtcherine, V., and Tsang, D. C. W. (2022). “Biochar as construction materials for achieving carbon neutrality,” *Biochar* 4(1), 1-15. DOI: 10.1007/s42773-022-00182-x

Article submitted: April 5, 2023; Peer review completed: April 20, 2023; Revised version received and accepted: April 27, 2023; Published: May 5, 2023.

DOI: 10.15376/biores.18.3.4492-4509